

Numerical evidence of quantum melting of spin ice: quantum-classical crossover

Yasuyuki Kato¹ and Shigeki Onoda^{1,2}

¹*RIKEN Center for Emergent Matter Science (CEMS), Wako, Saitama 351-0198, Japan*

²*Condensed Matter Theory Laboratory, RIKEN, Wako, Saitama 351-0198, Japan*

(Dated: September 21, 2022)

Unbiased quantum Monte-Carlo simulations are performed on the simplest case of the quantum spin ice model, namely, the nearest-neighbor spin- $\frac{1}{2}$ XXZ model on the pyrochlore lattice with an antiferromagnetic longitudinal and a weak ferromagnetic transverse exchange couplings, J and J_{\perp} . On cooling across $T_{\text{CSI}} \sim 0.2J$, the specific heat shows a broad peak associated with a crossover to a classical Coulomb liquid regime characterized by a remnant of the pinch-point singularity in longitudinal spin correlations as well as the Pauling ice entropy for $|J_{\perp}| \ll J$, as in classical spin ice. On further cooling, the entropy restarts gradually decaying to zero for $J_{\perp} > J_{\perp c} \sim -0.103J$, as expected for bosonic quantum Coulomb liquids. With negatively increasing J_{\perp} across $J_{\perp c}$, a first-order transition occurs at a nonzero temperature from the quantum Coulomb liquid to an XY ferromagnet. Relevance to magnetic rare-earth pyrochlore oxides is discussed.

PACS numbers: 02.70.Ss, 75.30.Kz

A compact U(1) gauge theory hosts dual electric and magnetic monopoles as well as photons, as emerge in non-Abelian gauge theories for grand unified theories [1, 2]. In condensed matter, it is expected to appear in a nearest-neighbor spin- $\frac{1}{2}$ XXZ model (or its variant) on the pyrochlore lattice [3–5], given by a simple Hamiltonian,

$$\mathcal{H} = \sum_{\langle \mathbf{r}, \mathbf{r}' \rangle} [J s_{\mathbf{r}}^z s_{\mathbf{r}'}^z + J_{\perp} (s_{\mathbf{r}}^x s_{\mathbf{r}'}^x + s_{\mathbf{r}}^y s_{\mathbf{r}'}^y)], \quad (1)$$

with an spin- $\frac{1}{2}$ operator $\mathbf{s}_{\mathbf{r}} = (s_{\mathbf{r}}^x, s_{\mathbf{r}}^y, s_{\mathbf{r}}^z)$ at a pyrochlore lattice site \mathbf{r} , and the nearest-neighbor longitudinal (z) and transverse (xy) exchange couplings $J (> 0)$ and J_{\perp} . This model gives the most simplified case of low-energy effective spin models for prototypical magnetic rare-earth pyrochlore oxides, defined in the C_2 -invariant local spin frames with their z axes pointing inwards to or outwards from the center of the tetrahedron [6–8]. These oxides include, for instance, $\text{Pr}_2\text{Ir}_2\text{O}_7$ [9], $\text{Pr}_2\text{Zr}_2\text{O}_7$ [6, 7, 10], $\text{Yb}_2\text{Ti}_2\text{O}_7$ [8, 11, 12], and $\text{Tb}_2\text{Ti}_2\text{O}_7$ [7, 13–17], all of which show vital roles of quantum effects due to nonzero J_{\perp} .

The particular limit $J_{\perp} = 0$ of the model is reduced to the nearest-neighbor classical spin ice (CSI) model. It involves a macroscopic degeneracy of the ground states satisfying the 2-in, 2-out spin ice rule [18, 19] and the Pauling residual entropy $S_{\text{P}} = \frac{1}{2} \ln \frac{3}{2}$ [20], as observed in $\text{Ho}_2\text{Ti}_2\text{O}_7$ [19, 21] and $\text{Dy}_2\text{Ti}_2\text{O}_7$ [22]. This CSI has been well understood in terms of a classical Coulomb phase physics in a gauge theory on the dual diamond lattice [4, 23, 24]: the Hamiltonian is given by $\frac{J}{2} \sum_{\mathbf{R}_{\sigma}} n_{\mathbf{R}_{\sigma}}^2$ with the static gauge charge, $n_{\mathbf{R}_{\sigma}} = \sigma \sum_{\mu=0, \dots, 3} s_{\mathbf{R}_{\sigma} + \sigma \mathbf{b}_{\mu}}^z$, defined at the center \mathbf{R}_{σ} of the tetrahedron, where $\sigma = \pm$ and \mathbf{b}_{μ} denote the sublattice index of the diamond lattice and the four nearest-neighbor diamond lattice vectors, respectively. The population of this gauge charge, dubbed a spin ice monopole [24], vanishes with decreasing temperature and the spin correlations become the dipolar

form [23], indicating deconfined monopoles.

In the simplest quantum spin ice (QSI) model (1) with nonzero J_{\perp} , on the other hand, the gauge charge acquires a quantum kinematics as bosonic spinons carrying spin- $\frac{1}{2}$ and playing a role of scalar Higgs fields in the U(1) gauge theory [25]. This kinematics completely lifts the degeneracy of the spin ice manifold. A degenerate perturbation theory about J_{\perp} yields a bosonic U(1) quantum spin liquid having deconfined dual gauge charges and linearly dispersive gapless “photons” [3]. This prediction was partially tested by quantum Monte-Carlo (QMC) simulations [5] which found a consistency of the spin correlations with those of “photons” for small J_{\perp} at low temperatures, while the bosonic U(1) quantum spin liquid is replaced by negatively large J_{\perp} with an XY ferromagnet. For a pure lattice U(1) gauge model obtained by projecting Eq. (1) onto the spin ice manifold, a variational Monte-Carlo study at zero temperature showed a finite-size scaling of the total energy that is consistent with the “photons” [26].

On the other hand, finite-temperature properties remain controversial. There have been experimental observations of a decrease of the entropy below S_{P} at very low temperatures in $\text{Dy}_2\text{Ti}_2\text{O}_7$ [27], $\text{Yb}_2\text{Ti}_2\text{O}_7$ [28], $\text{Pr}_2\text{Zr}_2\text{O}_7$ [10], and $\text{Pr}_2\text{Ir}_2\text{O}_7$ [29], some of which are most likely ascribed to an onset of a crossover from CSI to QSI. Recent large- N mean-field calculations for the $O(N)$ matter field coupled to the gauge field based on Wilson’s idea [30] proposed a possibility of a finite-temperature first-order phase transition of the resonating valence bond type that does not break any physical symmetry [31]. However, this approximation violates Elitzur’s theorem prohibiting a broken local gauge invariance [32]. In this regards, unbiased calculations for finite-temperature properties of even the simplest quantum spin ice model have been called for.

In this Letter, we reveal a finite-temperature phase diagram of the simplest QSI model (1), uncovering two

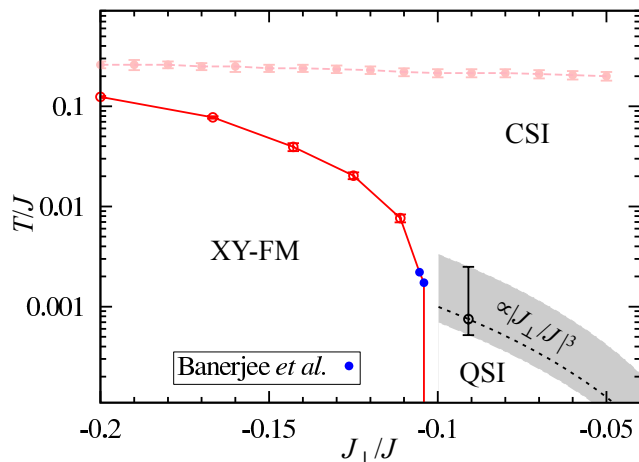


FIG. 1: (Color online) Finite-temperature phase diagram for $J_{\perp} < 0$, obtained with QMC simulations. Below the phase boundary (solid line) the transverse (xy) component of spins are ferromagnetically ordered, i.e., the order parameter (s^+) and the stiffness ρ_S are both finite. The blue dots are extracted from Ref. [5]. The dashed lines indicate the crossover temperatures estimated from the position of the broad peaks in specific heat curves.

successive crossovers and a single first-order phase transition shown with dashed and a solid lines in Fig. 1. From a high-temperature side, the system first crosses over to a classical Coulomb liquid or CSI regime with the entropy approximating to the Pauling entropy, and then for small enough $|J_{\perp}/J|$, to a quantum Coulomb liquid or QSI regime where the Pauling entropy is gradually released to zero. For $J_{\perp} < J_{\perp c}$ with $J_{\perp c}/J = -0.103$ [5], a first-order phase transition occurs to an XY-ferromagnet (XY-FM) [5].

All the numerical results presented in this Letter are obtained with unbiased worldline QMC simulations based on the path integral formulation in the continuous imaginary time [33]. To update worldline configurations, we adopt a directed-loop algorithm [34] in the $\{s_r^z\}$ basis, with the modification previously introduced for softcore bosonic systems to reduce the computational cost [35]. To moderate the freezing problem often arising in frustrated systems, we employed the thermal annealing, i.e., the temperature is gradually decreased in the simulations. We performed typically ~ 10000 Monte-Carlo sweeps for each temperature.

Let us start with the disordered side $J_{\perp} > J_{\perp c}$ of the phase diagram. Figure 2 shows for $J_{\perp}/J = -1/11$ the temperature dependence of (a) the energy density $\varepsilon \equiv \langle \mathcal{H} \rangle / N_s$ with $N_s (= 4 \times L^3)$ being the total number of spins, (b) the specific heat $C \equiv \partial \varepsilon / \partial T$, and (c) the entropy $S \equiv \log 2 - \int_T^{T_{\max}} (C/T) dT$ with $T_{\max} = 50/11$. We find two successive crossovers that are signaled by two broad peaks in the specific heat at $T_{\text{CSI}} \sim 0.2J$ and $T_{\text{QSI}} \sim |J_{\perp}^3/J^2|$. The higher-temperature crossover is

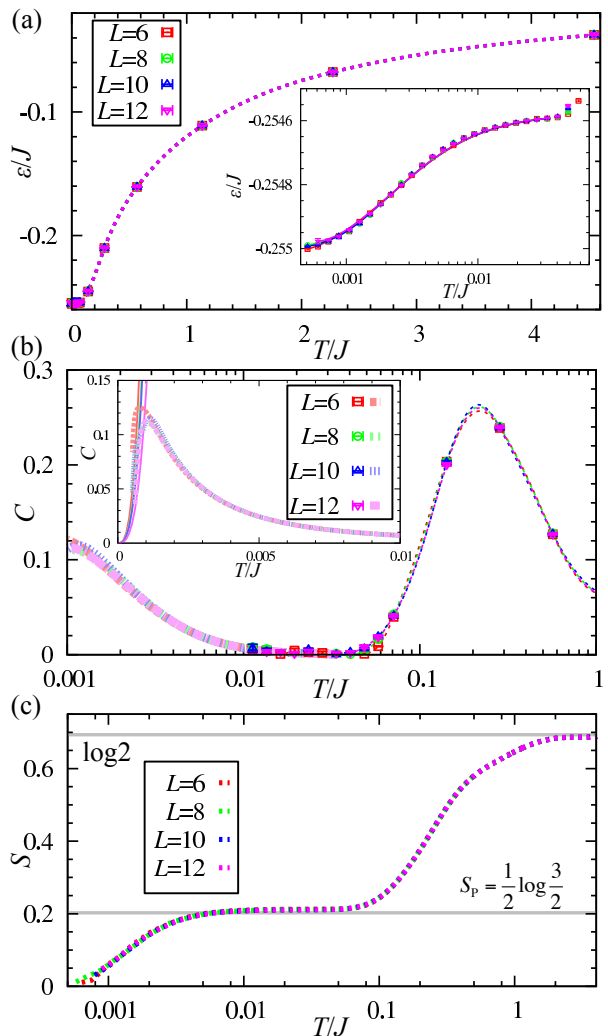


FIG. 2: (Color online) Temperature dependence of (a) the energy density ε , (b) the specific heat $C \equiv \partial \varepsilon / \partial T$, and (c) the entropy S for $J_{\perp}/J = -1/11 > (J_{\perp}/J)_c$. Dashed and solid lines in (a) are obtained through the cubic and the basis spline interpolation of the QMC data, respectively. The wider lines in (b) correspond to the numerical derivative of the basis spline functions of ε . The thinner solid lines in the inset of (b) are the fits to $C_{\text{photon}} = \frac{a^3 \pi^2}{15c^3} T^3$.

from a high-temperature local-moment regime with the entropy of the order of $\log 2$ to a classical Coulomb liquid or CSI regime where the entropy gradually decays to the spin ice plateau S_P as shown in Fig. 2 (c). On further cooling across T_{QSI} , the specific heat C shows an upturn, gradually releasing the Pauling entropy, indicating that the spin ice is melted by quantum fluctuations [6] and the system crosses over to a quantum Coulomb liquid or QSI regime. The lowest-energy excitations of the quantum Coulomb liquid are linearly dispersive “photons”, which describe a gauge-charge-0 harmonic oscillator mediating coupled transverse and longitudinal spin fluctuations [3]. Assuming the dispersion

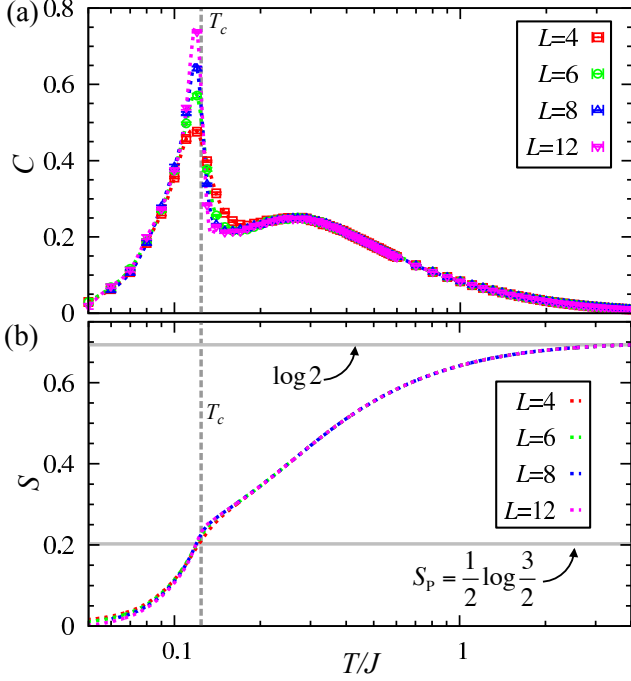


FIG. 3: (Color online) Temperature dependence of (a) C and (b) S for $J_{\perp}/J = -1/5 < (J_{\perp}/J)_c$. Dashed lines are the cubic spline interpolation of the QMC data in (a). The entropy is computed from the cubic spline interpolation of the specific heat data with $T_{\max}/J = 4$.

$\varepsilon_{\text{photon}}(\mathbf{k}) \sim c|\mathbf{k}|$, the density of states is computed as $D(\varepsilon) = \frac{2}{4} \left(\frac{a}{2\pi}\right)^3 \int d^3\mathbf{k} \delta(\varepsilon - c|\mathbf{k}|) = \frac{\varepsilon^2 a^3}{4\pi^2 c^3}$, where a is the cubic lattice constant, and the two polarizations and the four FCC primitive unit cells inside the cubic unit cell have been taken into account. Thus for $T \ll |J_{\perp}^3/J^2|$, the energy density is derived from this density of states as $\varepsilon \simeq \frac{a^3 \pi^2}{60c^3} T^4 + \text{const.}$, leading to the specific heat of “photons”, $C_{\text{photon}} = \frac{a^3 \pi^2}{15c^3} T^3$. The speed of “light” c is estimated by fitting the QMC data of the energy density at $T/J < 0.001$ as $c \simeq (1.3 \pm 0.2)ag\hbar^{-1}$ for $J_{\perp}/J = -1/11$ where $g \equiv |3J_{\perp}^3/(2J^2)|$. This value lies between $c = (1.8 \pm 0.1)ag\hbar^{-1}$ for $J_{\perp}/J = -1/9.7$ [5] and $c = (0.6 \pm 0.1)ag\hbar^{-1}$ in the limit of $|J_{\perp}/J| \rightarrow 0$ [36].

The higher temperature crossover to the CSI regime at $T_{\text{CSI}} \sim 0.2J$ is also observed in the case of $J_{\perp} < J_{\perp,c}$, as marked with (red) dashed line in Fig. 1. To be explicit, it is demonstrated for $J_{\perp}/J = -1/5 < (J_{\perp}/J)_c$ in Fig. 3 (a). The entropy S computed from the specific heat C (Fig. 3 (b)) resembles the case of $J_{\perp}/J = -1/11 > (J_{\perp}/J)_c$, except that the plateau at the Pauling entropy in the CSI regime is masked by the spiky peak in C due to a ferromagnetic transition at $T_c/J = 0.124(3)$.

Next, we clarify the spin correlations on the disordered side. Figures 4 present the energy-integrated \mathbf{Z} -polarized neutron-scattering cross-sections $\sigma_{\text{SF}}(\mathbf{q}) \equiv \sigma_{\text{T}}(\mathbf{q}) - \sigma_{\text{NSF}}(\mathbf{q})$ in the spin flip channel, except the nu-

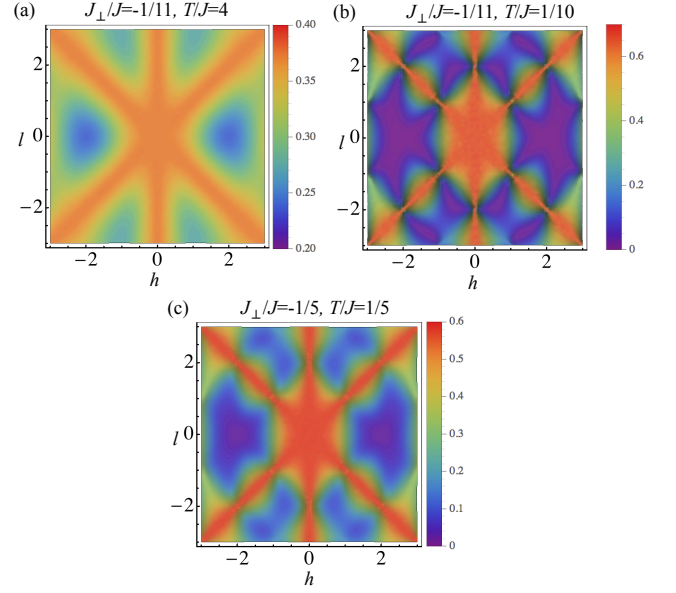


FIG. 4: (Color online) Spatial profiles of the energy-integrated polarized magnetic neutron-scattering cross-sections in the spin-flip channel, obtained with the QMC simulation at $L = 24$; (a) $J_{\perp}/J = -1/11$ and $T/J = 4$, (b) $J_{\perp}/J = -1/11$ and $T/J = 1/10$, and (c) $J_{\perp}/J = -1/5$ and $T/J = 1/5$. The wave vector is given by $\mathbf{q} = (2\pi/a)(h, h, l)$, and neutron spins are assumed to be polarized along $\mathbf{Z} = (1, -1, 0)/\sqrt{2}$.

clear form factor, where

$$\begin{aligned} \sigma_{\text{T}}(\mathbf{q}) &\equiv \sum_{\mu, \mu'} \langle s_{\mu}^z \mathbf{q} s_{\mu'}^z - \mathbf{q} \rangle \left\{ \hat{\mathbf{b}}_{\mu} \cdot \hat{\mathbf{b}}_{\mu'} - (\hat{\mathbf{b}}_{\mu} \cdot \hat{\mathbf{q}}) (\hat{\mathbf{b}}_{\mu'} \cdot \hat{\mathbf{q}}) \right\}, \\ \sigma_{\text{NSF}}(\mathbf{q}) &\equiv \sum_{\mu, \mu'} \langle s_{\mu}^z \mathbf{q} s_{\mu'}^z - \mathbf{q} \rangle \left\{ \hat{\mathbf{b}}_{\mu} \cdot \mathbf{Z} - (\hat{\mathbf{b}}_{\mu} \cdot \hat{\mathbf{q}}) (\mathbf{Z} \cdot \hat{\mathbf{q}}) \right\} \\ &\quad \times \left\{ \hat{\mathbf{b}}_{\mu'} \cdot \mathbf{Z} - (\hat{\mathbf{b}}_{\mu'} \cdot \hat{\mathbf{q}}) (\mathbf{Z} \cdot \hat{\mathbf{q}}) \right\}, \\ s_{\mu\mathbf{q}}^z &\equiv \frac{1}{L^{3/2}} \sum_{\mathbf{R}_+} s_{\mathbf{R}_+ + \mathbf{b}_{\mu}/2}^z e^{i\mathbf{q} \cdot (\mathbf{R}_+ + \mathbf{b}_{\mu}/2)}, \end{aligned}$$

with $\mathbf{Z} \equiv (1, -1, 0)/\sqrt{2}$, $\hat{\mathbf{b}}_{\mu} \equiv \mathbf{b}_{\mu}/|\mathbf{b}_{\mu}|$, and $\hat{\mathbf{q}} \equiv \mathbf{q}/q$. A broad scattering intensity along the [100] and [111] rods appears at high temperatures $T > T_{\text{CSI}}$, e.g., for $J_{\perp}/J = -1/11$ at $T/J = 4$ (Fig. 4 (a)), as experimentally observed in $\text{Pr}_2\text{Zr}_2\text{O}_7$ [10] and well above T_c in $\text{Yb}_2\text{Ti}_2\text{O}_7$ [11, 12]. In the CSI regime, we clearly see remnants of the pinch-point singularity [23] at every reciprocal lattice vectors except at $\mathbf{q} = (0, 0, 0)$, both for $J_{\perp}/J = -1/11 > (J_{\perp}/J)_c$ at $T/J = 0.1$ (Fig. 4 (b)) and for $J_{\perp}/J = -1/5 < (J_{\perp}/J)_c$ at $T/J = 0.2$ (Fig. 4 (c)), as observed in $\text{Dy}_2\text{Ti}_2\text{O}_7$ [37] and $\text{Ho}_2\text{Ti}_2\text{O}_7$ [38]. In fact, the pinch point cannot evolve into a real singularity, because the 2-in, 2-out ice rule is dynamically violated by the spin-flip processes of Eq. (1) [6]. Unfortunately, the current algorithm did not provide a sufficiently good statistics for $\sigma_{\text{SF}}(\mathbf{q})$ at lower temperatures,

i.e., in the QSI regime. We note that the non-spin-flip channel $\sigma_{\text{NSF}}(\mathbf{q})$ always gives just a featureless constant.

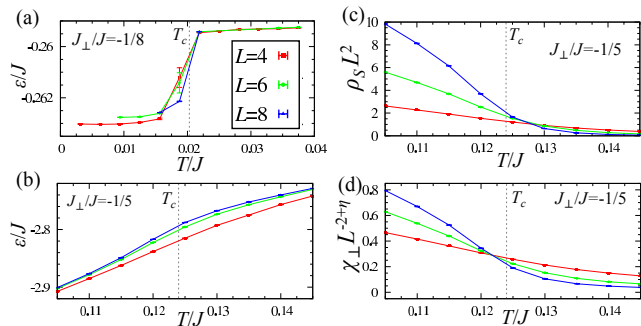


FIG. 5: (Color online) Determination of transition temperature. The energy density ε for $J_{\perp}/J = -1/8$ (a) and for $J_{\perp}/J = -1/5$ (b). The spin stiffness ρ_S (c) and the uniform transverse spin susceptibility χ_{\perp} scaled by $L^{-2+\eta}$ (d) for $J_{\perp}/J = -1/5$, with the critical exponent $\eta = 0.038$ for the 3D XY universality class [39].

Now we focus on the case of $J_{\perp}/J < J_{\perp c}/J = -0.103$, where a phase transition occurs to the XY-FM [5]. The transition temperature increases with negatively increasing J_{\perp} , as shown with the solid curve in the phase diagram (Fig. 1). When J_{\perp} is close to $J_{\perp c}$, the energy density $\varepsilon \equiv \langle H \rangle / N_s$ exhibits a clear discontinuous jump, as shown for $J_{\perp}/J = -1/8$ in Fig. 5(a), which gives the first-order transition temperature $T/J = 0.020(2)$. On the other hand, with negatively increasing J_{\perp}/J , the jump becomes less clear within our linear system sizes $L = 4, 6, 8$, as shown for $J_{\perp}/J = -1/5$ in Fig. 3(b). In this case, we just observe a sharp specific heat peak gradually growing with L (Fig. 3(c)) and crossings of the transverse spin susceptibility χ_{\perp} (Fig. 5(c)) and the spin stiffness ρ_S (Fig. 5(d)) at different L 's, where

$$\chi_{\perp} \equiv \frac{1}{\beta N_s} \int_0^{\beta} d\tau \sum_{\mathbf{r}} \langle s_{\mathbf{r}}^x(\tau) s_{\mathbf{0}}^x(0) \rangle,$$

$$\rho_S \equiv \frac{8\sqrt{2}}{3\beta |J_{\perp}| N_s} \langle \mathbf{W}^2 \rangle,$$

with the total winding number of worldlines \mathbf{W} [40]. In fact, the finite-size scaling does not hold in this case within our linear system sizes $L = 4, 6, 8$, as is seen from slightly different crossing temperatures of ρ_S and scaled χ_{\perp} , as shown in Figs. 5(c) and (d). Hence, we cannot conclude whether the transition is of either the weak first order or the second order in the case of $J_{\perp}/J \leq -1/6$. Then, the transition temperature in Fig. 1 is estimated from the average of the two crossing temperatures, while the error is from the difference. Note that this transition temperature also reasonably coincides with the specific heat peak temperature.

In principle, no classical spin models can describe the physics down to zero temperatures. Even so-called dipole-

lar spin ice such as $\text{Dy}_2\text{Ti}_2\text{O}_7$ and $\text{Ho}_2\text{Ti}_2\text{O}_7$ should involve quantum effects though it may be weaker than the energy barrier introduced by a crystal disorder. At a first glance, this may freeze the quantum kinematics of monopoles, making it harder to reach the QSI regime. Nevertheless, in the deconfined regime, spinons propagate nearly freely but are only affected by a Coulomb force. Such motions are hardly affected by dilute defects, since it is possible to find paths avoiding defects. Therefore, we expect very careful experiments taking into account a long thermal relaxation time possibly find a QSI regime with the entropy reduced from the Pauling ice entropy, as recently reported in $\text{Pr}_2\text{Zr}_2\text{O}_7$ [10] and $\text{Dy}_2\text{Ti}_2\text{O}_7$ [27]. In this regard, it is in principle possible to observe “photons” through microwave experiments. Note also that a similar entropy release has also been observed in another prototype of QSI, $\text{Pr}_2\text{Ir}_2\text{O}_7$ [29], which involves strong spin-orbit coupled Ir 5d conduction electrons and turns into a chiral spin liquid [9].

$\text{Yb}_2\text{Ti}_2\text{O}_7$ involves stronger quantum effects, as its ground state is given by a nearly collinear ferromagnet which is a Higgs phase in the context of a compact Abelian Higgs model for QSI [25, 28, 31]. However, even in this case, the spin correlation above T_c can exhibit a remnant of the pinch-point singularity, as found in our numerics on the simplest nearest-neighbor QSI model as well as in experiments and more directly relevant model [28]. Remarkably, the behaviors of the specific heat and the entropy shown in Fig. 3 resemble the experimental finding in $\text{Yb}_2\text{Ti}_2\text{O}_7$ [28], even though a realistic model includes bilinear coupling between the longitudinal and transverse spin components [8, 11, 12], which distorts the long-range ordered structure. In fact, the entropy at T_c in $\text{Yb}_2\text{Ti}_2\text{O}_7$ is below the Pauling entropy, unlike in our case, even though there is no spin-ice plateau [28]. These comparisons suggest that $\text{Yb}_2\text{Ti}_2\text{O}_7$ slightly above T_c is possibly only at an onset to a narrow, if any, QSI regime. Therefore, it is unlikely to observe “photons” in $\text{Yb}_2\text{Ti}_2\text{O}_7$.

We note that recent experiments on $\text{Tb}_2\text{Ti}_2\text{O}_7$ [16] have revealed a phase diagram which looks compatible with our result, including a quantum phase transition between a spin liquid and an ordered phase, except that our transverse spin order is interpreted as a quadrupole order [7, 25].

Acknowledgements: The authors thank M. Hermele for stimulating discussions. Numerical calculations were conducted on the RIKEN Integrated Cluster of Clusters. This work was partially supported by Grants-in-Aid for Scientific Research under Grant No. 26800199 and No. 24740253 and by the RIKEN iTHES project. S.O. acknowledges the hospitality of the Aspen Center for Physics supported by the National Science Foundation under Grant No. PHYS-1066293, and the hospitality of Nordita, Nordic Institute of Theoretical Physics, during his stays at the end of the work.

-
- [1] G. 't Hooft, Nucl. Phys. B **79**, 276 (1974).
- [2] A. Polyakov, JETP Lett. **20**, 194 (1974).
- [3] M. Hermele, M. P. A. Fisher, and L. Balents, Phys. Rev. B **69**, 064404 (2004).
- [4] R. Moessner and A. Ramirez, Phys. Today **59**, 24 (2006).
- [5] A. Banerjee, S. V. Isakov, K. Damle, and Y. B. Kim, Phys. Rev. Lett. **100**, 047208 (2008).
- [6] S. Onoda and Y. Tanaka, Phys. Rev. Lett. **105**, 047201 (2010).
- [7] S. Onoda and Y. Tanaka, Phys. Rev. B **83**, 094411 (2011).
- [8] S. Onoda, J. Phys.: Conf. Series **320**, 012065 (2011).
- [9] Y. Machida, S. Nakatsuji, S. Onoda, T. Tayama, and T. Sakakibara, Nature **463**, 210 (2010).
- [10] K. Kimura, S. Nakatsuji, J. Wen, C. Broholm, M. Stone, E. Nishibori, and H. Sawa, Nature communications **4**, 1934 (2013).
- [11] K. A. Ross, L. Savary, B. D. Gaulin, and L. Balents, Phys. Rev. X **1**, 021002 (2011).
- [12] L.-J. Chang, S. Onoda, Y. Su, Y.-J. Kao, K.-D. Tsuei, Y. Yasui, K. Kakurai, and M. R. Lees, Nature communications **3**, 992 (2012).
- [13] J. S. Gardner, B. D. Gaulin, A. J. Berlinsky, P. Waldron, S. R. Dunsiger, N. P. Raju, and J. E. Greedan, Phys. Rev. B **64**, 224416 (2001).
- [14] I. Mirebeau, P. Bonville, and M. Hennion, Phys. Rev. B **76**, 184436 (2007).
- [15] H. R. Molavian, M. J. P. Gingras, and B. Canals, Phys. Rev. Lett. **98**, 157204 (2007).
- [16] T. Taniguchi, H. Kadowaki, H. Takatsu, B. Fåk, J. Ollivier, T. Yamazaki, T. J. Sato, H. Yoshizawa, Y. Shimura, T. Sakakibara, et al., Phys. Rev. B **87**, 060408 (2013).
- [17] S. H. Curnoe, Phys. Rev. B **88**, 014429 (2013).
- [18] J. Bernal and R. Fowler, J. Chem. Phys. **1**, 515 (1933).
- [19] M. J. Harris, S. T. Bramwell, D. F. McMorrow, T. Zeiske, and K. W. Godfrey, Phys. Rev. Lett. **79**, 2554 (1997).
- [20] L. Pauling, *The Nature of the Chemical Bond* (Ithaca, NY: Cornell University Press, 1960).
- [21] S. T. Bramwell and M. J. P. Gingras, Science **294**, 1495 (2001).
- [22] A. P. Ramirez, A. Hayashi, R. Cava, R. Siddharthan, and B. Shastri, Nature **399**, 333 (1999).
- [23] S. V. Isakov, K. Gregor, R. Moessner, and S. L. Sondhi, Phys. Rev. Lett. **93**, 167204 (2004).
- [24] C. Castelnovo, R. Moessner, and S. L. Sondhi, Nature **451**, 42 (2008).
- [25] S. B. Lee, S. Onoda, and L. Balents, Phys. Rev. B **86**, 104412 (2012).
- [26] N. Shannon, O. Sikora, F. Pollmann, K. Penc, and P. Fulde, Phys. Rev. Lett. **108**, 067204 (2012).
- [27] D. Pomaranski, L. Yaraskavitch, S. Meng, K. Ross, H. Noad, H. Dabkowska, B. Gaulin, and J. Kycia, Nature Physics **9**, 353 (2013).
- [28] L.-J. Chang, M. R. Lees, I. Watanabe, A. D. Hillier, Y. Yasui, and S. Onoda, Phys. Rev. B **89**, 184416 (2014).
- [29] Y. Tokiwa, J. J. Ishikawa, S. Nakatsuji, and P. Gegenwart, Nature Materials **13**, 356 (2014).
- [30] K. G. Wilson, Phys. Rev. D **10**, 2445 (1974).
- [31] L. Savary and L. Balents, Phys. Rev. B **87**, 205130 (2013).
- [32] S. Elitzur, Phys. Rev. D **12**, 3978 (1975).
- [33] N. Kawashima and K. Harada, J. Phys. Soc. Jpn. **73**, 1379 (2004).
- [34] O. F. Syljuåsen and A. W. Sandvik, Phys. Rev. E **66**, 046701 (2002).
- [35] Y. Kato, T. Suzuki, and N. Kawashima, Phys. Rev. E **75**, 066703 (2007).
- [36] O. Benton, O. Sikora, and N. Shannon, Phys. Rev. B **86**, 075154 (2012).
- [37] D. J. P. Morris, D. A. Tennant, S. A. Grigera, B. Klemke, C. Castelnovo, R. Moessner, C. Czternasty, M. Meissner, K. C. Rule, J.-U. Hoffmann, et al., Science **326**, 411 (2009).
- [38] T. Fennell, P. P. Deen, A. R. Wildes, K. Schmalzl, D. Prabhakaran, A. T. Boothroyd, R. J. Aldus, D. F. McMorrow, and S. T. Bramwell, Science **326**, 415 (2009).
- [39] M. Campostrini, M. Hasenbusch, A. Pelissetto, P. Rossi, and E. Vicari, Phys. Rev. B **63**, 214503 (2001).
- [40] E. L. Pollock and D. M. Ceperley, Phys. Rev. B **36**, 8343 (1987).